Role of Buoyancy and Heat Release in Fire Modeling, Propagation, and Instability

Shahid M. Mughal[1], Yousuff M. Hussaini[2], Scott L. Goodrick[3], and Philip Cunningham[2]

Abstract—*In an investigation of the dynamics of coupled fluid-combustion-buoyancy driven problems, an idealised model formulation is used to investigate the role of buoyancy and heat release in an evolving boundary layer, with particular emphasis on examining underlying fluid dynamics to explain observed phenomena arising in forest fire propagation. The role played by the Froude number and background ambient wind in affecting various characteristics observed in propagating fires is addressed. A simplified flow situation is modeled in which controlled amounts of volumetric heat is injected into the system. By varying the strength of the heat source and the ambient winds the study examines the impact of these variables on the flow dynamics and the consequential development of instability waves that may provide insight into environmental conditions that contribute to erratic fire behaviour. Analysis suggests that there are two routes to fire behaviour and destabilisation, with Froude number playing a crucial role in the boundary layer development and consequential instability of the convecting flow. In low Froude number situations, the mechanism of fire induced local winds may arise as a product of heat release and buoyancy, which induces favourable pressure gradients accelerating local winds to above the ambient. The analysis shows that a massive destabilisation takes place and that stationary, zero streamwise and nonzero spanwise wavenumber, viscous disturbances have the highest growth rates. These stationary spanwise vortex disturbances, commonly referred to as pure vortex longitudinal "roll cell" modes, might well be linked to cross roll features that have been identified in some recent fire related numerical simulations. The simple model shows that a key requirement in breakup of the fireline, is a low enough ambient wind. In high Froude number cases, the most probable factor is the sensitivity of the boundary layer to separate and lift off the surface; this being caused by massive updrafts of buoyant air. The relatively weak nature of instabilities in this regime suggests that the convecting fireline development would otherwise be well behaved.*

In: Butler, Bret W.; Cook, Wayne, comps. 2007. The fire environment—innovations, management, and policy; conference proceedings. 26-30 March 2007; Destin, FL. Proceedings RMRS-P-46CD. Fort Collins, CO: U.S. Department of Agriculture, Forest Service, Rocky Mountain Research Station. 662 p. CD-ROM.

[1] Research Associate, Institute for Mathematical Sciences, Imperial College, London, UK. s.mughal@imperial.ac.uk

[2] Professor of Mathematics, with School of Computational Science, and Assistant Professor with Department of Meteorology, respectively, Florida State University, Tallahassee.

[3] Research Meteorologist, U.S. Department of Agriculture, Forest Service, Southern Research Station, Athens, GA.

Introduction

Our concern is with combustion related problems, in particular forest fires, where intense volumetric heat and mass release arise during the burning process. This is a complex process whereby entrainment and mixing lead to chemical reaction, release of heat, and mass, which in turn affect the flow dynamics and hence flow entrainment, mixing and combustion; that is, the effect of one on the other is coupled and may be cyclic. It is now fairly well recognised through observations that fire propagation characteristics fall into two distinct categories. For weak wind conditions, the fire front is mainly

affected by the expansion of the hot gases around the combustion zone, and in the literature this wildfire propagation regime is identified as plume dominated. For greater wind speeds the flame trajectory is affected more so by the lateral wind flow, and hot gasses are pushed toward the unburnt solid fuel, inducing additional heat source/release points.

To understand the effect of heat release on this quite complex process, we examine a simplified flow situation in which controlled amounts of volumetric heat is injected into the system. By varying the strength of our heat source and the ambient winds, we seek to examine the impact of these variables on the flow dynamics and the consequential development of instability waves that may provide insight into environmental conditions that contribute to erratic and dangerous fire behaviour.

An evolving fire is of course a complex flow, involving flow unsteadiness, turbulence, thermo-dynamics, multiple phases, chemistry, radiative effects and fluid dynamic coupling. These physical mechanisms are generally considered too complex, outside of a research environment, to be integrated on a large scale to simulate fire spread. Thus, present day fire spread models simplify the problem by representing the fire front as a curve separating the burnt area and the fresh fuel. Each point of this front is regarded as a possible ignition source (provided conditions are right), with normally empirical and experimentally derived formulae used to continue the computations to the next time and spatial level (Rothermel 1972). At the other level of sophistication, and requiring considerable computational resources, we cite the work of Morvan and Dupuy (2004), who model a wildfire propagation process by a complete multiphase formulation, though due to computational expense this work was limited to two dimensions. Typically such works model the full burning process, and thus include thermal degradation, pyrolysis, glowing combustion of solid fuel particles, convection, radiative heat transfer, effects of external wind and ground topography. Furthermore to be as realistic as possible, the solid fuel (that is, the natural vegetation) is further broken down into families of solid combustible particles, with each family (pine needles, twigs, foliage, excelsior, and so forth) characterised by a set of physical properties (density, flammability, moisture content, and so forth), which are also included in their mathematical model. A similar approach that allows for fully three-dimensional simulations of coupled atmosphere-fire behaviour, albeit employing a simplified treatment of combustion, is found in the work of Linn (1997) and Linn and Cunningham (2005).

Real fire observations and model simulations have shown that intense vortices of various strengths and sizes often occur; vortices being created either directly by the fire front or by and in conjunction with atmospheric convection. Fire vortices on the scale of metres continually occur at the fire front and are an essential component of the convection, and are hypothesised to play a fundamental role in the physics of fire spread. Heat and moisture supplied through the burning of ground, canopy, and/or crown fuel during a forest fire generate extreme levels of buoyancy. The horizontal buoyancy gradients have in certain fire conditions produced vortices of tornado strength (Banta and others1992). The presence of vertical shear in the ambient atmosphere is also an important component of fire behaviour. Vertical shear is associated with horizontal vorticity that may be converted into vertical vorticity near the ground via tilting by updrafts in the vicinity of the fire, thus leading to highly nonuniform winds near the fireline. Cunningham and others (2003) further suggest that this vertical vorticity is associated with low level horizontal winds on the downstream side of the fire that are oriented in the opposite direction to the fire spread. Simulations of Clark and others (1996a) lend

support to this observation and confirm that presence of low-level wind shear can lead to particularly active fire behaviour. Moreover, the presence of low level negative shear (that is, winds decreasing with height near the ground) has been shown to be a common feature of so-called blowup fires (Byram 1954). The other feature of note is that winds at the fire scale can either be strongly modified or even solely produced by the fire, depending on the atmosphere-fire coupling. This coupling or feedback may occur over spatial scales from tens of metres at the flame front to kilometres on the scale of the total burn area. The magnitude and direction of the wind near the ground has been observed to play a crucial role in wildland fire spread.

The potential for erratic fire behaviour arising from buoyancy associated with large wildfires and horizontal flow was first theorised by Byram (1954). This theory centred upon the notion that erratic fire behaviour (instability) becomes more likely as the conversion rate of buoyant energy surpasses the flux of kinetic energy by the horizontal flow; hence, the idea of power of the fire versus the power of the wind. Byram's original theory was limited, however, by its assumptions of a neutral atmosphere and a nonentraining plume. Nelson (2003) extended the original work of Byram to remove these assumptions. A limitation of this work is that the problem is not posed as a coupled system with heat release influencing the development of the flow. Clark and others (1996a,b) make use of a numerical atmospheric model coupled to a simple fire spread model to investigate the influence of convective processes on fireline dynamics in a fully coupled system. This study provided strong evidence for a linkage between the convective Froude number F_o^2, and erratic fire behaviour, such as fingering of the fireline and the development of fire whirls of near tornado strength. Experiments were conducted for a range of wind speeds (1, 2, 3 and 5 m/s) and two fireline lengths (420 and 1500 m). These variations in wind speed accounted for a range of Froude numbers. For small values of F_o^2 they encountered strong coupling between the atmosphere and fire with erratic fireline behaviour. However, they did not delve into the nature of the instabilities. Thus, vortex tilting and unpredictability of ground winds are not only a hazard in itself to nearby firefighters, who have on occasions reported being toppled to the ground unpredictably by fire whirls, but are an important fire spread mechanism through both local dynamics and the ability to loft flaming objects into areas well removed from the fire front. The precise mechanisms of how these effects occur are still poorly understood.

This paper represents the starting point in a systematic investigation of the dynamics involved in the investigation of coupled fluid-combustion-buoyancy driven problems. In the present investigation, the basic objective of our work is to isolate the roles of the convective Froude number F_o^2 and volumetric heat release on fire dynamics and the nature of two and three dimensional unstable disturbances that arise. Most previous work is almost all based on the low temperature Boussinesq assumption, while detailed simulations use combinations of either fully unsteady compressible DNS and or large-eddy simulation (LES) models with combustion treated completely or approximated somehow. With such complex simulations, considerable difficulty arises in trying to isolate the underlying physics. Among the many reasons are the large amount of data that require processing and assimilation, and the computational expense of examining a large enough parameter space to isolate the role of key parameters. The model we use to examine the issues raised above is by way of examining the mixed forced-free convection boundary layer problem, which has been much studied in the past from the viewpoint of the heat-transfer problem. We contend and show below that this simple model

can be used to elucidate some major aspects of fire propagation phenomenon too. In particular, we are interested in situations where sizable changes occur in density, temperature, and transport properties due to heating. Thus, the commonly used approximation, used in most analytic and related numerical computations, of using a Boussinesq approximation is dispensed with, and we consider the fully coupled problem where temperature variations of the order of 1200K may arise.

In this paper we define the appropriate model and discuss our numerical work for the basic nonsimilar steady field, in which we incorporate the effects of a volumetric heat source and coupled buoyancy model. Results are discussed in the context of forest fire propagation and in view of existing knowledge of fire related phenomena. Flow instability aspects of the work are discussed by the use of *linear stability theory* (LST) briefly as we believe that a proper investigation of this aspect requires the effects of nonparallelism to be included, and LST does not allow this in a straightforward manner. But the preliminary instability analysis reported here does allow and will serve as a bedrock for a future and fuller investigation using the more advanced linear and nonlinear instability analysis tools. The work we believe is an important step in elucidating the coupling of the external fluid (or wind-driven) processes and the burning process and how the two interact. Our simplification of the problem describes the two major mechanisms of importance in a coupled fluid-combustion-buoyancy dominated problem, namely the role of heat release and Froude number on atmospheric dynamics and instability. Features such as fireline length and its effect on fire spread and propagation are effectively three-dimensional in nature and left for a later investigation.

The tools currently used operationally in the wildland fire community to predict fire spread are based on empirical relationships between ambient wind speed, topography, and fuel properties (Nobel and others 1980; Rothermel 1972). The complexities of the combustion process and the intricacies of fire-atmosphere feedback processes are largely neglected. The primary focus of such tools is on predicting the spread of wind driven surface fires (Froude number >1) under homogenous, steady state conditions. These models are not typically applicable to the most intense forest fires (crown fires). The model presented in the current work, with its boundary layer approximation, is well suited to providing a simplified vision of the problem based on physics rather than empirically derived relationships. The importance of the physics based relationship is that it allows us to explore the response of the system as we move toward more buoyancy dominated conditions. While the boundary layer assumption precludes application of the model to buoyantly dominated flows, it does allow for an initial, though limited, exploration of the transition from wind to buoyancy dominated conditions and the potential for associated instabilities. Examination of the initial stages of the transition from wind to buoyancy dominated conditions (and associated flow instabilities) provides insight into the conditions that will cause current operational tools to fail.

Formulation

Basic Steady Field

We consider the fully compressible two-dimensional flat plate natural convection problem that incorporates the Boussinesq assumption, namely that density variations may be ignored in all terms apart from the gravitational term, and we use the equation of state $p^* = \rho^* R^* T^*$ to determine density. Thus,

the relevant equations of mass conservation, momentum, and energy to determine the basic boundary layer state are:

$$\begin{aligned}
&\frac{\partial(\bar{\rho}\bar{U})}{\partial x}+\frac{\partial(\bar{\rho}\bar{V})}{\partial y}=0,\\
&\bar{\rho}(\bar{U}\frac{\partial\bar{U}}{\partial x}+\bar{V}\frac{\partial\bar{V}}{\partial y})=-\frac{\partial\bar{P}_e^{(o)}}{\partial x}-\frac{\partial\bar{P}^{(1)}}{\partial x}+\frac{\partial}{\partial y}(\bar{\mu}\frac{\partial\bar{U}}{\partial y}),\\
&\frac{\partial\bar{P}^{(1)}}{\partial y}=(\bar{\rho}_e-\bar{\rho})g^*,\\
&\bar{\rho}(\bar{U}\frac{\partial\bar{T}}{\partial x}+\bar{V}\frac{\partial\bar{T}}{\partial y})=\frac{\bar{U}}{C_p}(\frac{\partial\bar{P}_e^{(o)}}{\partial x}+\frac{\partial\bar{P}^{(1)}}{\partial x})+\frac{1}{\sigma}\frac{\partial}{\partial y}(\bar{\mu}\frac{\partial\bar{T}}{\partial y})+\frac{\bar{\mu}}{C_p}(\frac{\partial\bar{U}}{\partial y})^2+\bar{Q}(x,y,z).
\end{aligned}\tag{1.1}$$

$\bar{P}_e^{(o)}(x)$ is the flow induced pressure field, and we introduce the function $\bar{Q}(x,y,z)$ to represent the volumetric heat release that arises from a burning fire. In the above x and y are streamwise and wall normal coordinates, $\bar{U},\bar{V}$ the associated velocities, $\bar{\rho}$ the density, $\bar{T}$ the temperature, $\bar{\mu}$ the viscosity, C_p the specific heat, σ the Prandtl number, and g^* the gravitational term.

To reduce the equations into a more suitable form for numerical work, we transform y using a Falkner-Skan type transformation

$$\eta=(\frac{\bar{\rho}_e\bar{U}_e}{\bar{\mu}_e x})^{1/2}\int_0^y\frac{\bar{\rho}(s)}{\bar{\rho}_e}ds,\tag{1.2}$$

and $\psi=(\bar{\rho}_e\bar{\mu}_e\bar{U}_e x)^{1/2}f$ with ψ a stream function, which satisfies mass conservation. On assuming Mach number terms of $O(M^4)$ are negligible, the equations then reduce to

$$\begin{aligned}
&\frac{\partial(\chi f'')}{\partial\eta}+m_1(s-f'^2)+cff''-sx\frac{d\bar{P}^{(1)}}{dx}=x(f'\frac{\partial f'}{\partial x}-f''\frac{\partial f}{\partial x}),\\
&\frac{\partial\bar{P}^{(1)}}{\partial\eta}=x^{1/2}G_o(s-1),\\
&\frac{\partial}{\partial\eta}(\frac{\chi T'}{\sigma})+(\gamma-1)\chi M^2f''^2+cfT'+(\gamma-1)M^2sf'x\frac{d\bar{P}^{(1)}}{dx}+sx\hat{Q}(x,\eta)=x(f'\frac{\partial T}{\partial x}-T'\frac{\partial f}{\partial x}),
\end{aligned}\tag{1.3}$$

where

$$\chi=\frac{\bar{\mu}\bar{\rho}}{\bar{\mu}_e\bar{\rho}_e};m_1=\frac{x}{\bar{U}_e}\frac{d\bar{U}_e}{dx};c=\frac{1+m_1}{2}+\frac{1}{2}\frac{x}{\bar{\mu}_e\bar{\rho}_e}\frac{d}{dx}(\bar{\mu}_e\bar{\rho}_e);M^2=\frac{\bar{U}_e^{\,2}}{\gamma R^*\bar{T}_e}.$$

Here, $f'=\bar{U}/\bar{U}_e, T=\bar{T}/\bar{T}_e$ and $\bar{\rho}_e/\bar{\rho}=s$ and are all assumed to be functions of η and x; M is the streamwise edge Mach number and the viscosity $\bar{\mu}$ is allowed to behave according to Sutherland's law. The quantities $\bar{\rho}_e,\bar{U}_e,\bar{T}_e,\bar{\mu}_e$ are functions of the surface conforming coordinate x; however, in this work we only consider the case of uniform flow over a flat surface and as such $m_1 = 0$; $c = 1/2$.

The far-field boundary conditions are the usual ones of

$$f'(\eta\to\infty,x)=T(\eta\to\infty,x)=s(\eta\to\infty,x)=1;\bar{P}^{(1)}(\eta\to\infty,x),=0$$

while at the wall $\eta = 0$,

$$f(0,x) - f_w(x); f'(0,x) = 0;$$

and for temperature, either the wall temperature or adiabatic condition (of zero heat-transfer) can be satisfied, namely:

$$T(0,x) = \bar{T}_w(x) / \bar{T}_e(x) = T_m - \frac{T_b}{2}(1 + \tanh(\frac{x - x_s}{x_T}))$$

or

$$T'(0,x) = 0;$$

the subscript w refers to the wall value and f_w allows for wall suction or blowing (mass efflux) to be incorporated into the analysis.

In the above, the quantities of interest are the inverse of the Froude number defined

$$G_o = \frac{g^* L}{\bar{U}_e^2 R_L^{1/2}} \tag{1.4}$$

With L a length scale and $R_L = \bar{\rho}_e \bar{U}_e L / \bar{\mu}_e$ a Reynolds number, while the heat source term is dimensionalised as follows:

$$\hat{Q}(x,\eta) = \frac{L\bar{Q}(x,\eta)}{C_p \bar{U}_e \bar{T}_e}. \tag{1.5}$$

We note from (1.3) that the key parameter that controls the magnitude of the buoyancy effect is G_o, and if all other free parameters vary, it is this parameter that needs to be fixed to obtain similarity of solutions, when two apparently quite different flows are compared. Interpretation of the results and their relationship to length scales associated with real fires may be seen by associating the Sutherland viscosity model used presently with the subgrid-scale based eddy viscosity and diffusivity concepts (Deardorff 1973) used in LES based simulations. Observe that η in (1.2) involves the viscosity $\bar{\mu}_e$,as do the definitions of the inverse of the Froude number G_o (through the Reynolds number R_L). Thus, in principle by a simple association of the subgrid based eddy viscosity in these scalings, the results presented herein may be applied to the length scales associated with evolving fires, albeit rather crudely.

Source Formulation

Our ultimate objective is to consider quite general situations where the source function consists of a steady 3-D-forcing term and an unsteady component, namely

$$Q^*(x,y,z,t) = \hat{Q}(x,y,z) + \delta q(x,y,t) e^{i\beta z}$$

where $\delta << 1$. However, in this work we assume the source forcing to be steady only and of infinite extent in z (Cunningham and others 2003), having the form

$$\hat{Q}(x,y,z) = q_o \tanh(\frac{\bar{x}}{x_o}) \exp(-\frac{y - y_s}{y_o}) \exp(-(\frac{\bar{x} - \bar{x}_s}{x_L})^2) \tag{1.6}$$

with the parameters $q_o, x_o, y_o, y_s, \bar{x}_s, x_L$ chosen conveniently. A typical example is shown in figure 1a, while figure 1b shows a possible wall temperature distribution that may be enforced. This particular wall temperature form is used to model the fact that behind the fireline, temperatures will have been raised by the evolving fire, while ahead of the fireline surface temperatures are still presumed to be at ambient levels.

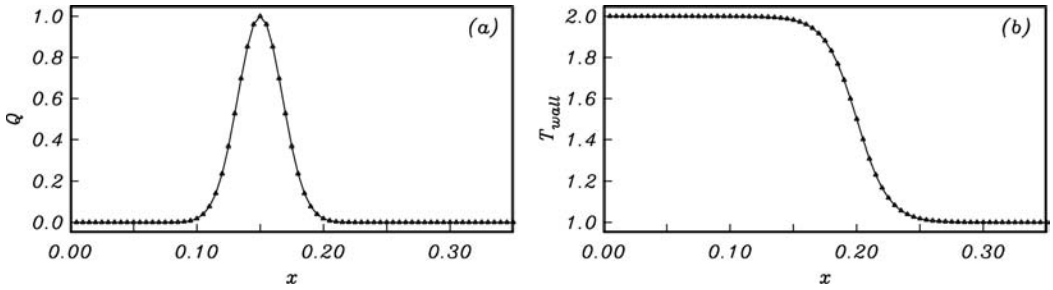

Figure 1—(a) Source strength distribution along the wall $y = 0$ for the parameters $q_o = 20$; $x_o = 0.001$; $y_o = 3$; $x_s = 0.15$; $x_L = 0.025$. (b) Wall temperature distribution for parameters $T_m = 2, T_b = 1, \bar{x}_s = 0.2, x_T = 0.025$ of equation 1.6.

Numerical Procedure

The system of equations are parabolic and thus solved by a fully implicit second-order accurate three-point backward differencing scheme, with a two point second-order accurate discretisation in the wall normal direction. The two point scheme arises by converting the second-order momentum and energy equations into a system of first-order equations. The nonlinear terms are discretised using standard Newton linearisation; thus, ultimately the inversion of a block tridiagonal matrix arises, which can be accomplished efficiently using standard methods. To initialise the computations at $x = 0$, the similarity form of (1.3) is used and thereafter a marching procedure employed.

For small magnitudes of $\hat{Q}$ the forced heat source problem will be amenable to a marching boundary layer type solution strategy. While as one should expect, and investigated by Higuera (1997), where sizable changes occur in the wall temperature, such a simple solution strategy will ultimately fail, in which case an interactive thermal layer with the pressure determined by the external inviscid adjustment of the boundary layer thickness needs to be computed or allowed for in any numerical scheme. Thus, either an interactive boundary layer type solution procedure or the fully Navier-Stokes solution procedure needs to be invoked. Flow reversal, separation, and reattachment regions do occur and are predicted by the asymptotic triple-deck analysis of Higuera (1997).

Daniels and Gargaro (1993) Boussinesq based buoyancy driven flow investigations conclude that in cases where the Froude number is too low, the boundary layer flow cannot be sustained, and the forward motion succumbs to the adverse pressure gradient induced by buoyancy. This either leads to the onset of reverse flow and the consequent failure of the numerical scheme or more generally to the occurrence of a terminal singularity. In cases where reverse flow sets in, their computations failed due to numerical instability rather than the existence of any local singular behaviour. The flow becomes subject to upstream influence, which then requires a much more sophisticated numerical treatment.

We examine the situation where both significantly raised temperatures and sizable buoyancy effects arise. Thus, at some stage where the flow parameters lead to a strong coupling between the normal pressure gradient and convective terms, either from significantly raised temperatures or buoyancy effects, we must anticipate a breakdown in the numerical solutions, since then the external inviscid field is strongly modified and straightforward boundary layer

theory can then no longer be expected to be valid. We restrict our analysis to the parameter regime, where the problem is amenable to a parabolic boundary layer marching type solution procedure; namely where $G_o \sim O(1)$. Ultimately, however, as the buoyancy effects become sizable, boundary layer solution technique used here will fail, and at this point recourse to a fully Navier-Stokes solution for computation of the underlying basic state has to be made.

Basic Flow Solutions

The basic state model to be investigated is that of the forced basic steady flow, with Froude number and volume heat source $\hat{Q}$ as competing/coupled effects. We only consider zero pressure gradient, low Mach number flows, with flow parameters $T_\infty = 300K, \sigma = 0.72, R_L = 10^5, L = 1\text{m}$. The computational domain is of extent $0 \le x \le 1$, with a step length in x of $\Delta x = 0.005$. To obtain variations in Froude number we vary the free stream velocity U_e, and generally in fire related problems these flow velocities are in the range 0.5 ~ 10m/s, though as alluded to earlier the key parameter that controls the flow structure is G_o as defined by (1.4). Typical temperature variations examinable are up to 1200K; this may be varied by changing the source strength q_o.

Zero Volume Source Strength, $\hat{Q}$, and Zero Buoyancy

We begin by presenting some results for the zero source strength, zero buoyancy case. Of course this problem is the trivial flat plate incompressible Blasius problem; however, this serves as a useful guide and comparator when the more interesting parameter regime results are presented. Figure 2a shows streamwise velocity U and its derivatives, while figure 2b the streamwise normal velocity $V = V' / U_e'$ distribution at various x-intervals. Since this has a similarity structure, as would be expected, the numerical solution for U at all x-positions is identical, while that for V shows a decrease in the transpiration velocity or efflux to the external inviscid stream as the flow progresses downstream. We note two things: (1) this is of relative small order (as expected) and (2) it attains uniformly constant value sufficiently far from the wall. Furthermore, since the wall temperature is specified to be identical to the ambient, temperature variations are negligible and are thus not shown. Figure 3 shows the effect of maintaining different, above the ambient, uniform wall temperatures on solutions. The boundary layer thickens, the wall shear decreases, and the normal velocity magnitude increases; however, the near-similarity structure in the U and T profiles is still found to persist.

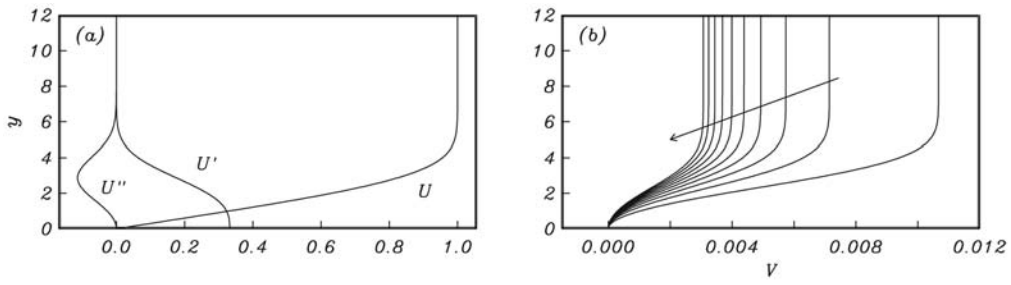

Figure 2—Blasius profiles at x = 0.065,(0.08),0.785 intervals. (a) Streamwise U velocity and derivatives U', U''. (b) Wall normal V velocity; arrow is in direction of increasing x.

To consider the effect of buoyancy on the solutions, we merely switch on the buoyancy terms in our equations and repeat the computations and the effect is shown in figure 3 by the dashed curves. We note that the differences are quite small, though they begin to increase as the wall temperature increases. The external wind speed for this particular run is approximately 3.46 m/s and the parameter $G_o = 1/386$; thus, one should not expect significant differences as the parameters selected are for a large Froude number.

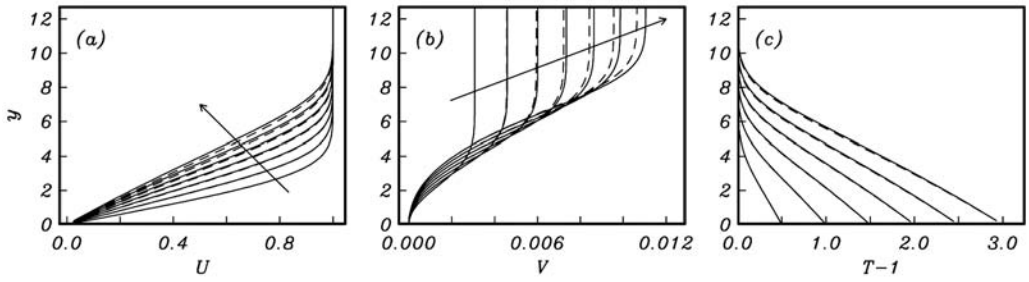

Figure 3—Compressible zero pressure gradient profiles at $x = 0.785$ for wall temperatures T_{wall} = (300,(150),1200), $T_\infty = 300K$, direction of arrows indicate increasing wall temperature. Comparison of solutions with (dashed line) and without (solid) inclusion of buoyancy terms in governing equations. (a) Streamwise *U* velocity; (b) Wall normal *V* velocity; (c) Temperature *T-1*.

Effects of Source Strength, $\hat{Q}$

We next consider how switching on the heat source affects results. We begin by examining the large Froude number case, corresponding to a wind speed of 10 m/s. The appropriate *Q*-source distribution selected is determined by trial and error; the particular source term distribution used here is that shown in figure 1a. Note from (1.6), that Y_o fixes the extent in y of the heat release, and choosing $y_o < 5$ essentially assumes that most of the heat release occurs within the boundary layer; setting $y_s > 0$ maximises the heat release off the wall boundary. The strength of the heat release (which determines the maximum temperature) is fixed by q_o. Figure 4a shows the temperature and figure 4b the wall normal (or updraft) velocity distributions achieved for varying q_o keeping y_o constant at various downstream positions. Apart from the obvious, namely increasing q_o increases boundary layer temperatures, we see that the effect is quite localised to the vicinity of the heat source (maximum heat release occurs at x=0.15). Observe that peak temperatures of about four times the ambient (~1200K) are achievable near the source, with the choice of parameters used. Downstream the overall temperatures decay in magnitude but still remain quite substantial.

We observe that changing the magnitude of the heat source has a major impact on affecting the magnitude of the vertical velocity. In the vicinity of the heat source maximum, a quite strong updraft of air arises for increasing q_o (note fig. 4b), but then immediately downstream of it a weaker though still relatively substantial downdraft also occurs. We note from figure 4b, for the choice of parameters or source forcing, the updraft velocity is almost 40 percent of the streamwise velocity, while the downdraft almost 10 percent. This downdraft diminishes, quite rapidly as we move downstream of the source, unlike the local temperature and streamwise velocity fields. We do compute

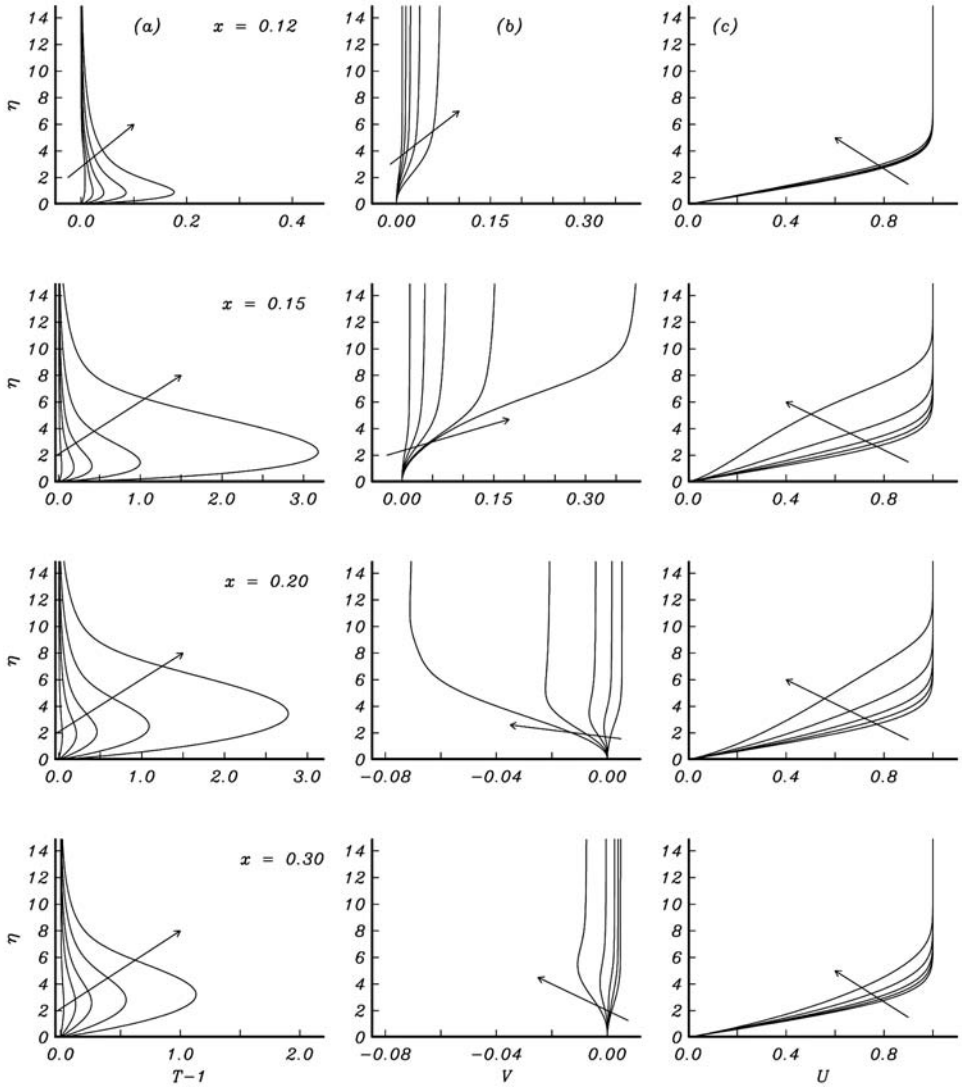

Figure 4—Effect of increasing source term magnitude q_o on nonbuoyancy driven flow at various x-locations. $U_e = 10m/s; q_o = (1,5,10,20,40); y_s = 0; y_o = 4; \bar{x}_s = 0.15; x_L = 0.025;$ $T_{wall} = T_\infty = 300K$ (*arrows point in direction of increasing* q_o). (a) Temperature profiles. (b) Wall normal velocity (*or updraft*) distributions. (c) Streamwise velocity distributions.

even greater updraft velocities for greater values of q_o which in fact exceed the value 1, with apparently no ill-effects as regards code convergence problems in this limit. We note that boundary layer theory, and the equations used presently are derived on assumption of $V \sim O(R_L^{-1/2})$, though the only terms omitted are the streamwise diffusion terms to render the equation parabolic and the assumption that the vertically convected momentum flux is of an order less than that induced by density changes. The mass conservation equation is solved exactly, so the only crucial weakness in the present model is that of assuming that the system is solvable by a parabolic marching procedure.

The effect of the heat source on the streamwise velocity, as may be deduced from figure 4c, is that heating modifies this quite drastically too, causing in general a reduction of the wall shear and a doubling of the boundary layer thickness. Ultimately if the applied heat release q_o is large enough, the boundary layer shows a tendency to separate. Our code in this limit then fails to converge. The above are computed for a ground temperature set to be the same as the ambient of $T_{wall} = T_\infty = 300K$, which is clearly impracticable; one

assumes real fires have ground temperatures significantly higher. We next set the wall temperature to $T_{wall} = 600K$ and repeat the above runs. This is seen more clearly in figure 5, which also shows the downstream development of the temperature profiles. Apart from the satisfaction of the higher wall temperature condition, generally the results and trends are unchanged from those presented in figure 4.

In the context of fire propagation and sustainability we observe that well ahead of the heat source (for example, $x \sim 0.3$ in fig. 4) temperatures of the order of 600K persist. It is precisely this feature that acts as a preigniter, which readies the source material for combustion ahead of the fire line. The above is a useful indicator, since the downwind propagation distance of a fire front is usually associated with the farthest downwind location where the temperature of the solid fuel is raised to a particular threshold to initiate or continue the burning process. This is also a criterion used in determining the *rate of spread* of the fire.

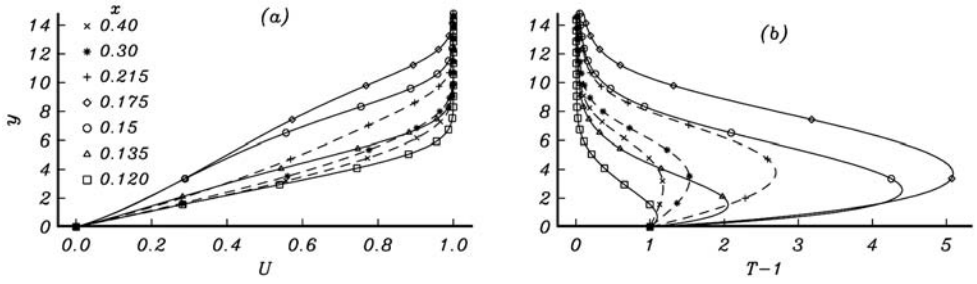

Figure 5—Streamwise velocity distributions at various x-locations. $q_o = 40$; $y_o = 4$; $y_s = 0$; $T_{wall} = 600K$; $T_\infty = 300K$. All conditions are identical to figure 4, except the wall temperature is held fixed at $600K$.

Buoyancy Effects

To examine buoyancy effects, based on evidence from the previous section, we choose values of $q_o = 25$, $y_o = 4$, $y_s = 0$ and gradually reduce the freestream velocity, thus reducing the effective Froude number F_o^2. As mentioned above it would appear to be more realistic to have sizable wall temperature and thus in all results presented we fix this at 600K. Moreover based on previous observations and numerical evidence gained presently, we note that the Froude number may be redefined to include temperature dependence, since we find numerical convergence of our fully coupled system of boundary layer equations is Froude number dependent. Thus, results are presented with the definition

$$\hat{F}_o^2 = \frac{\bar{U}_o^2 R_L^{1/2}}{L g^* \Delta T_{\max}}, \Delta T_{\max} = \frac{T_{\max}}{T_e} - 1, \qquad (1.7)$$

with T_{max} the temperature maximum in the boundary layer. This we note also follows from (1.3), since the term $\Delta T_{\max} / \hat{F}_o^2$ is the total magnitude of the buoyancy induced pressure component at any point in the field, and quite naturally the larger this becomes, the coupling between the equations

increases, until the system is no longer treatable using a parabolic based approach. Clark and others (1996a) in an attempt to characterise wind-driven fires use a similar expression, namely

$$\hat{F}_{rc}^2 = \frac{U_o^2}{W_f g^* \hat{\Delta} T_{\max}} \tag{1.8}$$

with $\hat{\Delta} T_{\max}$ a mean value of the temperature anomaly over the region of intense heating and W_f a fireline width in the mean wind direction. In the present case we observe that dynamical similarity between two different flows is assured provided the parameter G_o is identical. The cases examined and correspondence between U_e and $\hat{F}_o^2$ are given in table 1.

Table 1—Values of local Froude number $\hat{F}_o^2$ based on (1.7) for cases presented.

U_e (m/s)	$\hat{F}_o^2$	1 / G_o
10.00	1080	3224
7.50	610.5	1813
5.00	274.3	805.9
2.50	71.91	210.5
1.00	13.41	32.24
0.75	8.101	18.13
0.50	4.044	8.059
0.375	2.490	4.533
0.25	1.267	2.015
0.10	0.270	0.322
0.05	0.078	0.081

Profile distributions at a fixed Froude number (corresponding to $U_e = 0.05$ m/s) and varying the source strength q_o are shown in figure 6, while that of keeping q_o fixed and varying the Froude number are shown in figure 7. A number of important features may be deduced. The streamwise velocity develops distinct maxima; that is, inflectional profiles that exceed the freestream value of unity, before ultimately reducing back to unity for $y \to \infty$, and wind shear at the wall increases for decreasing $\hat{F}_o^2$. Normal velocity distributions near the heat source release are now downward directed (of order of about 30 percent), unlike the earlier high Froude number situation, followed by a much weaker updraft downstream of the heat source. This is almost the reverse of the situation depicted in figure 4. Temperature profiles show a reduction in magnitude for increasing buoyancy. Note a reduction in peak temperature of approximately 600K as the Froude number $\hat{F}_o^2$ reduces from 1080 to 0.078.

The generation of inflectional profiles is of course related to density (temperature) gradients and the high value of G_o that results in sizable buoyancy induced pressure gradients, which feed into accelerating the streamwise velocities by way of a strongly induced streamwise pressure gradient. In the earlier high Froude number situation this mechanism was suppressed, and thus the extra energy supplied in the form of the volumetric heat release could only be quickly dissipated by increasing the updraft velocity. Furthermore, we observe that inflectional profiles result from the temperature difference and that our inclusion of a heat release source term in the equations, simply

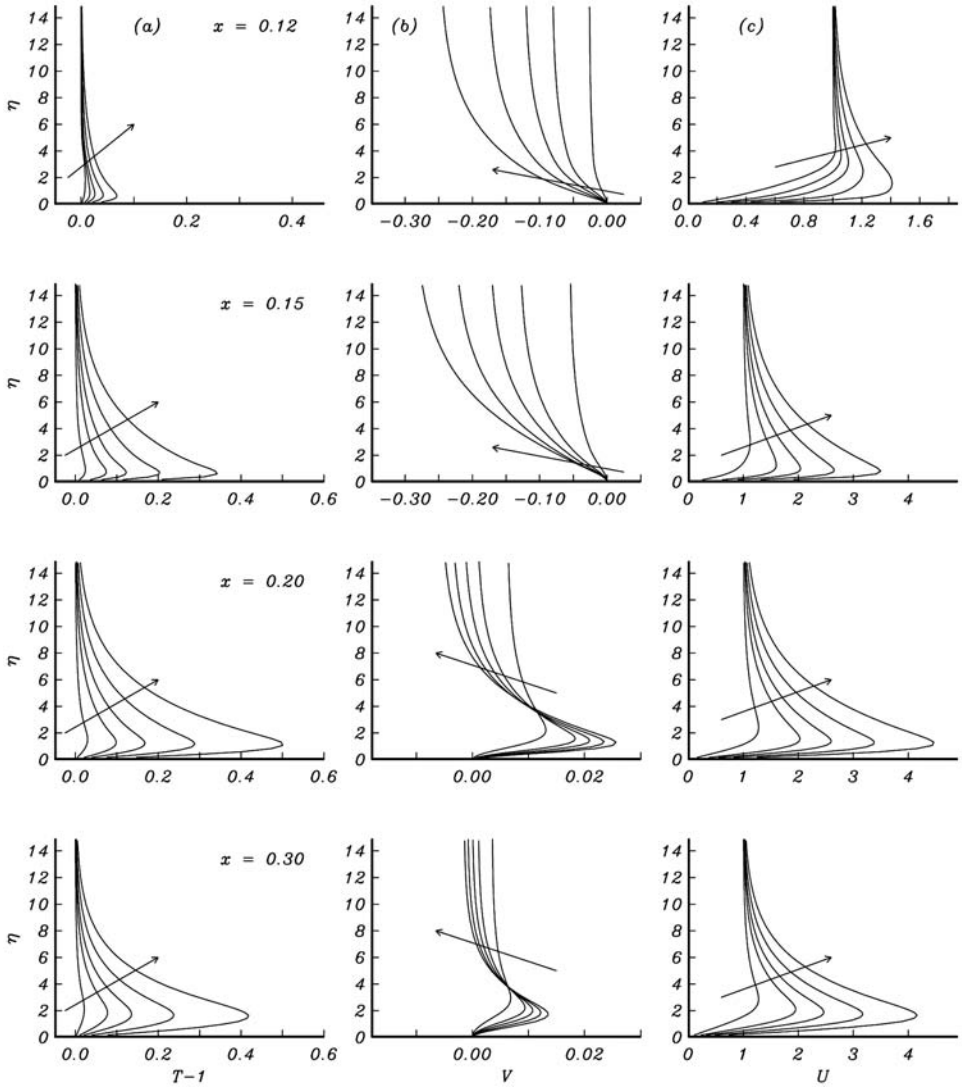

Figure 6—Effect of increasing source term magnitude q_o on basic buoyant flow at various x-locations. $U_e = 0.05m/s; q_o = (1,5,10,20,40); y_s = 0; y_o = 4; \bar{x}_s = 0.15; x_L = 0.025; T_{wall} = T_\infty = 300K$; (*arrows point in direction of increasing* q_o). (a) Temperature profiles. (b) Wall normal velocity (*or updraft*) distributions. (c) Streamwise velocity distributions.

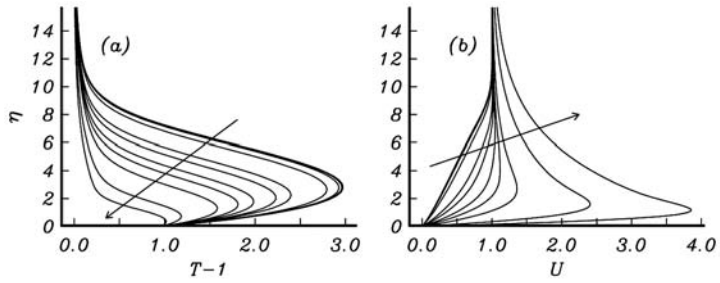

Figure 7—Profile distributions at $x = 0.175$ for varying Froude numbers corresponding to $U_e = (10.0,7.5,5.0,2.5,1.0,0.75,0.5,0.375,0.25,0.1,0.05)$ (*arrows point in direction of increasing* U_e). $q_O = 25$, $y_O = 4$, $T_{wall} = 600K$ (a) T temperature distributions. (b) U velocity distributions.

offers a facility to generate thermal variations in the boundary layer. In the absence of the heat source, inflectional profiles could have been generated by maintaining a different wall temperature from the ambient, and provided the Froude number (or $1/G_o$) is small enough, the same mechanism exists to generate inflectional profiles. The fact that inflectional profiles do not arise in figure 4 is that G_o is arranged to be of an almost negligible value, despite the fact that significant temperature differences (up to 900K) between the ambient and wall exist. To show that this is the case, figure 8 shows results for the case of maintaining uniform wall temperature at 600K, but computed for varying Froude numbers at a fixed position, and as expected inflectional profiles result for the low Froude number runs, and as indicated, thermal energy is used to accelerate the flow, thus resulting in less fuller temperature profiles compared to the high Froude number case.

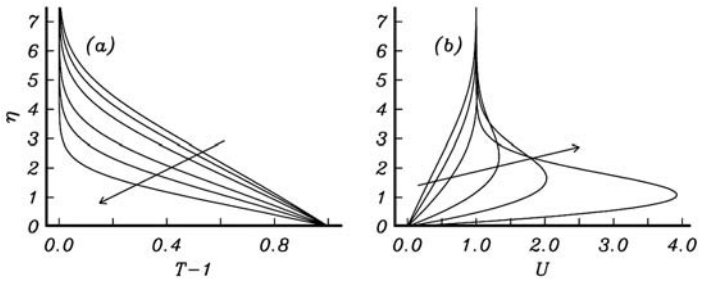

Figure 8—Profile distributions at $x = 0.3$ for varying Froude numbers corresponding to U_e = (10.0,0.5,0.25,0.1,0.05,0.02) (*arrows point in direction of increasing* U_e). Zero volumetric heat release; that is, $q_o = 0$, $T_{wall} = 600K$ buoyancy generated purely by maintaining a wall to ambient temperature difference. (a) T temperature distributions. (b) U velocity distributions.

The analogous case where, rather than the heated wall, the volumetric heat source produces the temperature difference is shown in figure 7. Observe that for low free-stream velocities the parameters $\hat{F}_o^2$ and G_o^{-1} in table 1 are similarly valued, while at high flow velocities this is not the case. This arises entirely from the fact that at low Froude numbers, as indicated in figures 6 and 7 and in relation to the earlier high Froude number results of figure 4, energy supplied in the form of heating is used to accelerate the streamwise velocity rather than raising field temperatures. Thus, in low Froude number situations the preference is for the thermal energy being utilised to accelerate the local flow, rather than raising temperatures. In the limit of extreme buoyancy, one then gets the situation where the flow quite aggressively uses as much of the heat energy in accelerating the local flow in the streamwise direction, leaving little in the temperature field.

The results of figure 6 are for an extreme value of the Froude number or an extremely buoyant flow, whereas in practise, provided the Froude number is of $O(1)$, one expects a tradeoff or competition between the propensity for the boundary layer to use the extra energy supplied by the heat source to either increase local boundary layer temperatures or locally accelerate the streamwise flow. This competition between the two is shown, for milder buoyancy driven case, in figure 9. In this case, free-stream velocity is about 0.5 m/s, and the effects of keeping the buoyancy fixed and increasing the heating through the source term are shown. We see a more typical situation

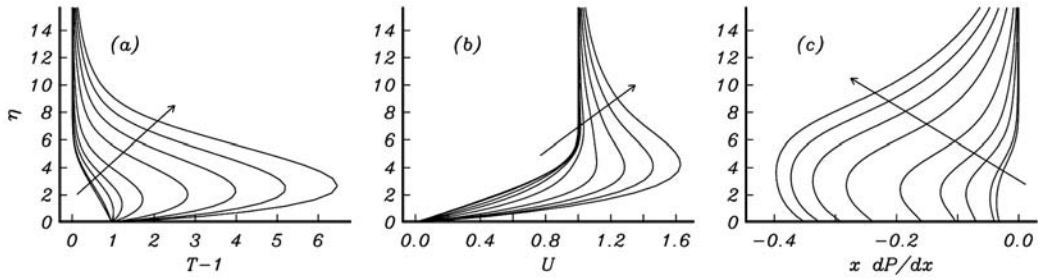

Figure 9—Profile distributions at $x = 0.175$ for fixed Froude number for varying source strength magnitude $q_o = (0,1,5,10,20,40,60,80,100)$ (*arrows point in direction of increasing* q_o). $U_e = 5m/\,s$, $y_o = 4$, $T_{wall} = 600K$ (a) T temperature distributions. (b) U velocity distributions. (c) Streamwise pressure gradient distributions.

that probably arises in fire situations, where both overshoots in the streamwise velocity and substantially increased temperature profiles arise. Figure 9c shows the induced pressure gradient, which is the factor in causing the acceleration of the streamwise flow.

The main point to note, however, is that the crucial parameter that governs the strength of the buoyancy is G_o, so the value of the ambient wind speed is immaterial and by appropriate choice of parameters—that is, viscosity or density say—a parameter situation can be created where buoyancy is a sizable factor, even though wind speeds may appear large.

Finally we present in figures 10 through 12 the main features uncovered in the analysis. Figure 10 shows temperature and streamwise velocity for a mildly buoyant flow, while figure 11 the case where the buoyancy is considerably stronger. In these computations we have also specified a wall temperature distribution shown in figure 1b; thus, beyond $x \sim 0.2$, the wall temperature is specified to be $300K$, while upstream it is fixed at 600K. We note the extreme velocity overshoot arising for the $U_e = 0.05$ case; these overshoots in velocity persist well downstream of the heat source as do the raised temperatures, in spite of the fact that the wall temperature is specified to be the ambient. As already noted, buoyancy terms effectively force or use the energy supplied by the heating to accelerate the streamwise velocity at the expense of increasing the temperature field. This additional acceleration of the flow stream (due to heating) thus forces the horizontal boundary layer motion to be sustained for a larger extent downstream before it ultimately succumbs to the adverse pressure gradient generated by the buoyancy. Presumably in situations of continuous applied heat source in the downstream direction, this motion may well then be self-sustaining.

We further note the quite concentrated and strong downdraft region in the vicinity of the heat source in figure 12 and the switch over from a strong downdraft to an equally strong updraft in varying Froude number from low to high. The occurrence of weak downdraft behind the fireline, followed by relatively stronger updraft ahead of the fireline, has also been found in LES simulations of Linn and Cunningham (2005). Cunningham and others (2003) find that the magnitude of the heat source is a major factor in the magnitude of the vertical velocity produced and then go on to suggest that this plays a key role in the amount of time it takes for a buoyant parcel to rise through the shear layer and that the counter rotating vortex pair observed in their simulations has its origin near the ground as a pair of vortices oriented

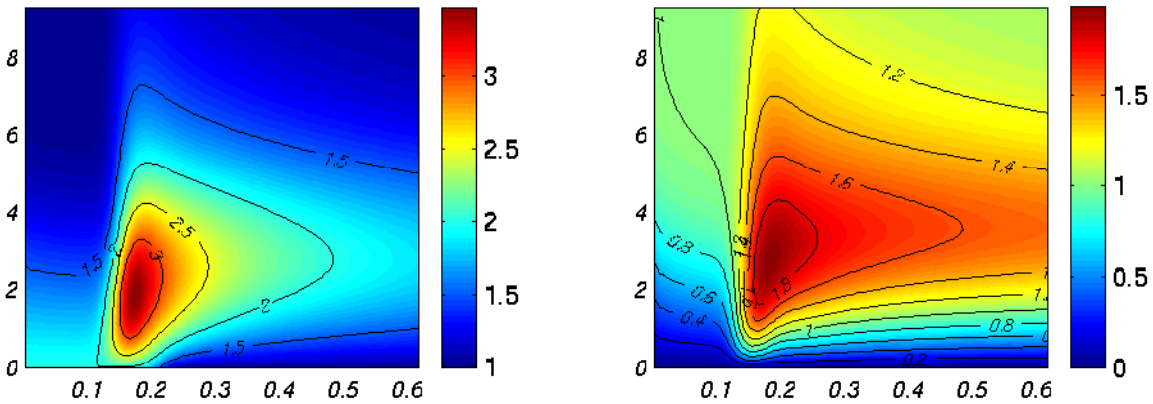

Figure 10—Mild buoyancy case corresponding to $U_e = 0.25$m/s; $y_O = 4$, $y_S = 2.0$, $q_O = 40$, $x_L = 0.05$, $T_{wall} = 600K$ (a) Temperature field. (b) Streamwise velocity field.

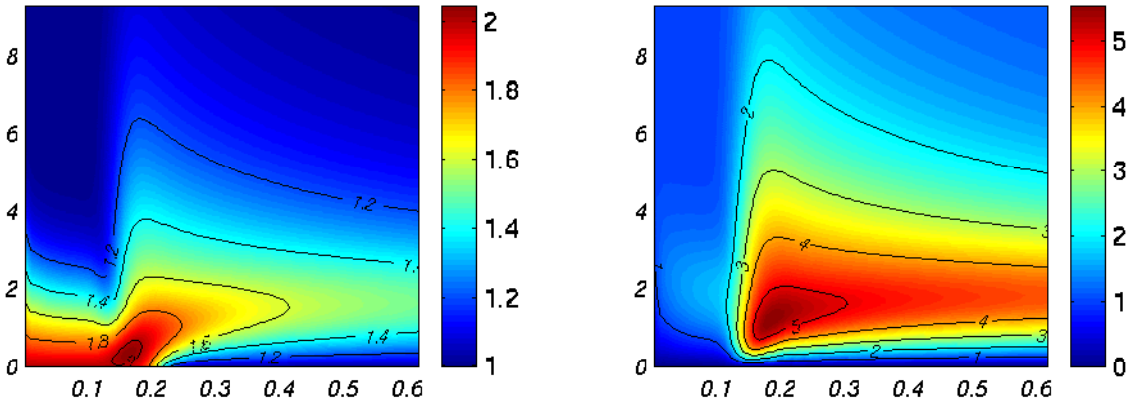

Figure 11—Strongly buoyant case corresponding to $U_e = 0.05$m/s; $y_O = 4$, $y_S = 2.0$, $q_O = 40$, $x_L = 0.05$, $T_{wall} = 600K$ (a) Temperature field. (b) Streamwise velocity field.

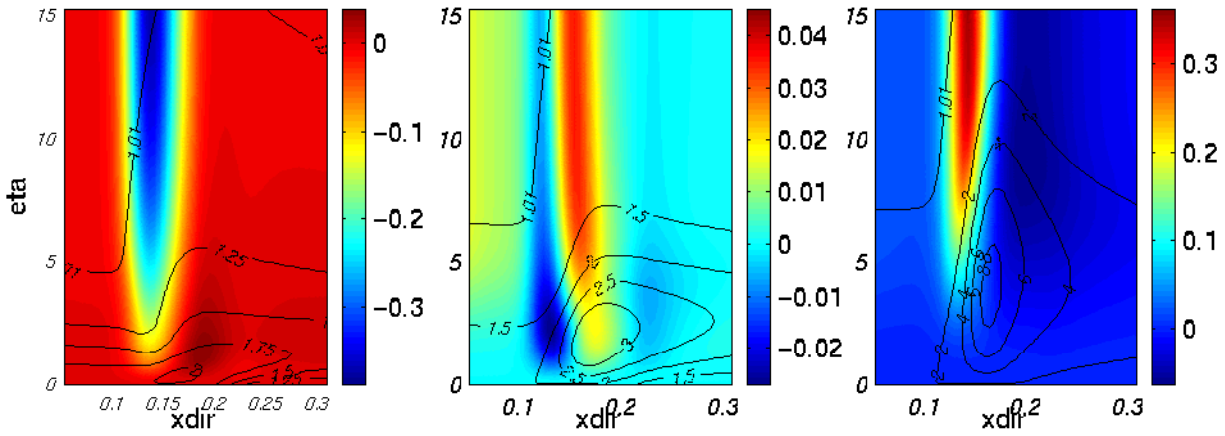

Figure 12—Wall normal velocity distribution for varying Froude number, for fixed source strength magnitude. Contours denote the superposed temperature field. (a) $U_e = 0.05$m/s; (b) $U_e = 0.25$ m/s, (c) $U_e = 2.5$ m/s. $q_O = 40$, $y_O = 4$, $T_{wall} = 600K$.

primarily in the vertical direction. Since buoyancy can only directly generate horizontal vorticity, the vertical vorticity can only be generated by tilting of the horizontal into vertical direction. In this regard, the strongly buoyant updraft plays a key role.

Cases where the streamwise velocity exceeds unity may play a role in the propagation of crown fires (fires burning through the tree canopy rather than through surface fuels). A recent observational study using infrared imagery to examine crown fire dynamics noted horizontal flows far greater than ambient winds by an order of magnitude (Coen and others 2004). They hypothesise that these bursts, as they refer to them, are the result of nonlinear interactions that transfer vertical momentum generated by buoyancy to horizontal momentum before buoyancy takes over and produces a more vertical plume rise. This theory would seem to be supported by the present work, in that we observe that the buoyancy term effectively forces or uses the energy supplied by the heating to accelerate the velocity.

Inflectional profiles have been noted before as being tied to extreme fire behaviour (Byram 1954).

However, the focus on the ambient wind profile is inflectional, not the input of heat generating an inflectional profile. The reasoning is that hot columns of rising air draw in air from the surroundings, thus leading to wind-induced acceleration of the local winds in the vicinity of the fire line. Clark and others (1996a) present cases of similar dynamics in a fully 3-D coupled model that produces significant fingering of the fireline in the spanwise direction at low Froude number values. They suggest that when the fireline's speed is slow enough, fire-generated winds break up the fireline. Though how this breakup occurs, from a rigorous physics or mathematical modeling viewpoint, is not addressed. They surmise that eventually convection and local dynamics become nonlinear, producing erratic shapes to both the fire line and convection. They hypothesise that large horizontal buoyancy gradients at the fire front produce strong horizontal vortices, and the vertical motions within the fire eventually lead to vortex tilting, producing vertical vorticity, and that in some cases these vertical vortices cause the breakup of the fireline. After breakup of the convection column, the formation of fingers is identified in the vicinity of the fire. They conclude that fire line breakup and formation of fingers are the result of light winds and thus a dynamically unstable fire line leading to the breakup of the two-dimensional column of hot air into multiple columns. Moreover, in addition to $\hat{F}_o^2$ being small, they conjecture that another ingredient required for fingering to occur is that of low-level negative shear, where the wind blows faster near the surface than just aloft. They suggest that this arises either from gust fronts, convective downdrafts and mountain valley flows, whereas our analysis shows that the fire itself can generate such inflectional flows. They speculate that dynamic fingering is caused by vertical tilting regions of intense horizontal negative shear at the fire front leading to narrow regions of high speed, hot air shooting out in front of the fire. This is a major process in fire spread on the micro-scale, which causes fires to jump as they spread.

Summary of Basic Flow Solutions

We have shown that using quite a simple two-dimensional model formulation, a wide variety of forced heat and buoyancy coupled problems can be examined. Adding in heat release by way of distributed heat release over a finite extent allows many of the basic features arising in fire propagation to be identified or captured. Our intention has been to strip away the

complexity of using fully unsteady DNS multiphase based formulations and solution techniques in favour of a more rudimentary formulation in order to identify the key mechanisms arising and playing a major role in observed fire propagation. As such the model does produce features that typically arise in fires. Namely velocity overshoots or so-called super velocities caused by the coupling of buoyancy and heat release near the ground. The model suggests that in the low Froude number regime, heat release is directly responsible for causing the local streamwise wind speeds to accelerate drastically. Strongly inflectional stream wise velocity profiles are generated; thus, we can expect the more dangerous (from a boundary layer instability viewpoint) inviscid instabilities to arise. The analysis in this regime also shows that regions of high shear arise close to ground and that temperature profiles are generated that have been observed in typical forest fires. The model also correctly predicts the generation of strong updraft velocity followed by a weaker downdraft, though a role reversal is also predicted, whereby in high wind conditions heat release causes highly buoyant updrafts of air, while in low Froude number regimes the reverse happens and an equally strong downdraft arises. The model is easily extended to properly three-dimensional volumetric forcing, thus allowing for buoyancy dependence in (x, z)-directions and thus would allow the effect of fire-length in the spanwise direction to be simulated at a fraction of the computational cost of full DNS investigations.

Our interest in this problem originally arose from the viewpoint of addressing the instability properties of velocity and temperature profiles that typically arise in fire problems. There does not appear to have been any systematic study of examining the stability properties of boundary layer profiles of the type that do occur in fire-related problems. In particular as may be noted from figures 4, 5, and 7, typically quite dramatic and sizable temperature profiles arise, and the combination with the inflectional velocity profiles does not appear to have been examined or quantified from a boundary layer instability viewpoint. Of course, inflectional velocity profiles and their instability properties are well known, but the issue of sizable temperature profiles and their combination with inflectional velocity profiles have to our knowledge not been the subject of any systematic investigation. Moreover, in the study of the high Froude number case, we have shown temperature profiles of the order of 1200K are generated. The stability properties at this high temperature, low Mach number regime are of interest from the viewpoint of erratic fire behaviour, propagation, and also from the viewpoint of how vertical rotors, rotating rolls, and intense vortices develop. As shown in computations in this paper, strong horizontal gradients in buoyancy near the surface produce strong horizontal vorticity. As the horizontal vorticity is tilted into the vertical by the fire updraft, intense vertical vorticity may develop where large buoyancy and horizontal gradients of the vertical wind coexist. As is well known, within fires there are small vortical structures on the millimetre scale that tightly bend the flame fronts, up to vortex structures on length scales of many metres. Simulations of plumes from line sources by Cunningham and others (2003) find that as the plume rises, it is bent downstream, and a regular array of steady perturbations develop in the cross-stream direction along the plume cap. As time progresses, the plume then undergoes a transition from its initial two-dimensional structure to an eventual three-dimensional one, with this transition being evident in a region far from the heat source. The vorticity field shows that initially the dominant vortical structure is the spanwise vortex tube associated with the plume cap; while at later times streamwise vortex tubes become dominant.

To initiate an understanding of such complex features, the basis for investigation is the use of linear stability theory to look at trends and identify features that do lead to those observed and hypothesised above. Previous instability work has been almost wholly based on buoyancy associated with the low temperature Boussinesq assumption. The majority of earlier studies have been confined to examine stability of vortex structures where the coupling between the energy and momentum fields is weak and the fluid density or compressibility essentially plays no role apart from introducing the buoyancy associated pressure term into the equations. Thus, few works have considered fully compressible nonsimilar boundary layers and their consequent instability of the boundary layer profiles where the coupling between the energy and momentum fields is strong. Our principal interest in the following is how the effects of buoyancy influences the stability of the basic flows discussed above, in a fully compressible problem.

Linear Instability of Basic Flow

To conduct a linear stability analysis of the flow, first the standard decomposition of the flow variables into a main flow component and an (infinitesimally) small disturbance is applied. That is the total flow $\mathbb{Z}'$ described by the exact unsteady fully compressible Naiver-Stokes equations can be split into a basic *steady* flow and an *unsteady* component, hence

$$\mathbb{Z}'(x,y,z,t) = \bar{\mathbb{Z}}(y) + \Pi'(x,y,z,t),$$

with $\bar{\mathbb{Z}} \gg \prod'$. In the present case only a 2-D and steady mean flow is assumed. On the other hand, the disturbances are assumed to be 3-D and thus can be written as

$$\Pi'(x,y,z,t) = \Pi(y)\exp^{i(\alpha x+\beta z-\omega t)}.$$

An eigenvalue problem arises and thus a dispersion relation of form

$$\mathbb{F}(\alpha,\beta,\omega,R_\delta,F_o^2) = 0$$

requires to be satisfied. We specify (β,ω) as free parameters, with (R_δ, F_o^2) flow dependent and solve for the spatial eigenvalue α. The objective is to map out the parameter space in β,ω,R_δ and F_o^2. We concentrate on two aspects: (1) the stability of profiles of typical form given by figures 4 and 5; (2) low Froude number coupled with the heat source basic flows of form given by figures 6 and 9.

Influence of Source Distribution, Zero Buoyancy

Neutral curves corresponding to figures 4 and 5 (T_{wall} = *300K* and T_{wall} = *600K* respectively) are shown in figure 13 for varying heat source magnitudes. We observe two effects: one is that increasing q_o increases the instability frequency envelope, and second, we see that the neutral curves (for a large enough value of q_o) are closed. That is, heat release first causes a local (or further) destabilisation of the flow, totally rearranging the flow structure, but this is beneficial in that downstream of the heat release, the flow is totally stabilised. For the T_{wall} = 600*K* simulation, the flow in the absence of the

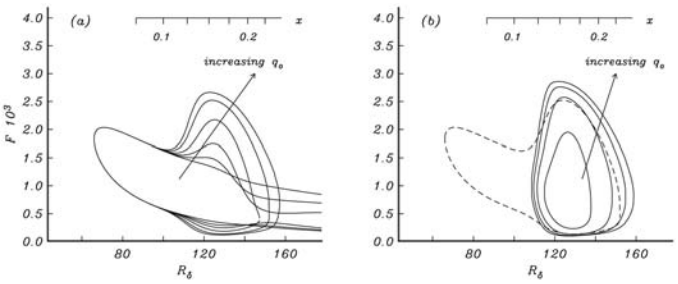

Figure 13—Zero buoyancy (U_e = 10 m/s) neutral curves for parameters of figures 5 and 4 for varying heat source magnitudes. $F = 10^3\ \omega\ /\ R_\delta$ m/is the circular frequency. (a) q_o = (1,5,10,20,40,60); $T_{wall} = 600K$. (b) q_o = (120,40,60,80); $T_{wall} = 300K$. Also superposed is the q_o = 40 result from figure (a) (*shown as dashed curve*).

volumetric heat source, becomes naturally unstable beyond $R_\delta \sim 66$; at about $R_\delta \sim 100$, corresponding to $x \sim 0.1$ (refer to fig. 1a), the instability envelope increases having its upper bound at about the point where peak heat is being released (x=0.15) and it then diminishes in size, and given the appropriate amount of heat the flow can be completely stabilised. Though not shown, further downstream we do find that as the flow readjusts to normalcy, the region of instability reappears, but this point can be shifted farther downstream by further increments in q_o. Of course q_o cannot be increased indefinitely, since ultimately the boundary layer shows a tendency to separate. But clearly we see that heat release causes a destabilisation of the flow in the vicinity of the heat source release region. These points are confirmed and reemphasised in the $T_{wall} = 300K$ case. In this case, heat is released well upstream in a region, which in normal circumstances exhibits no instability until about $R_\delta \sim 520$ (the critical Reynolds number for incompressible Blasius flow). Thus, heating generates the pocket of instability, and we further see that this is localised to the vicinity of the heat release region. Though not shown, the eigen-functions reveal that the unstable modes are thermally induced, in that temperature disturbances are the largest in magnitude. Though overall, the growth rates of these thermally induced unstable waves are found to be quite small.

Buoyancy Effects

Impact of decreasing Froude numbers on the neutral curves for 2-D disturbances is shown in figure 14a, while growth rates over the frequency span at various x positions for the lowest Froude number neutral curve, corresponding to U_e = 0.5m/s, are shown in figure 14b.We note that the U_e = 10.0m/s curve is closed and almost total stabilisation of flow is achieved, whereas for the lowest Froude number curve shown, the unstable frequency spectrum enlarges considerably in the heat release region while disturbances down to the stationary are unstable. In the limit of $\omega \to 0$ the growth rate and wavenumber both approach zero, while as $\omega \to \infty$ or large steamwise wavenumber limit, the disturbances ultimately return to being stable. Note that with increasing R_δ the growth rates increase substantially; thus, a rapid destabilisation occurs as a result of the heat release. Another feature is that as x increases the curves coalesce, and this may be due to the instability being essentially inviscid in structure, and so the value of R_δ becomes irrelevant.

Figure 15a shows growth rates for 3-D disturbances arising in the mildly buoyant flow examined in figure 14b and shows that in a certain frequency

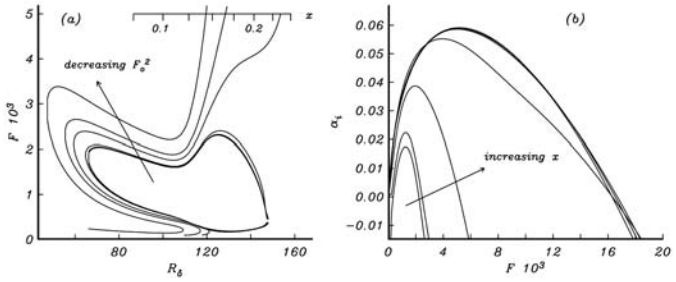

Figure 14—Neutral curves for increasing levels of buoyancy, computed for parameters corresponding to figure 7. Neutral curves are shown for Froude numbers corresponding to(U_e = 0.5, 0.75,1.0, 2.5,5.0,10.0); T_{wall} = 600K. (b) Amplification curves for varying frequency at various x-positions corresponding to the plot shown in (a) for the U_e = 0.5m/s case; arrow points in direction of increasing downstream distance in x corresponding to R_δ =100, 110,120, 130, 140, 150,158.

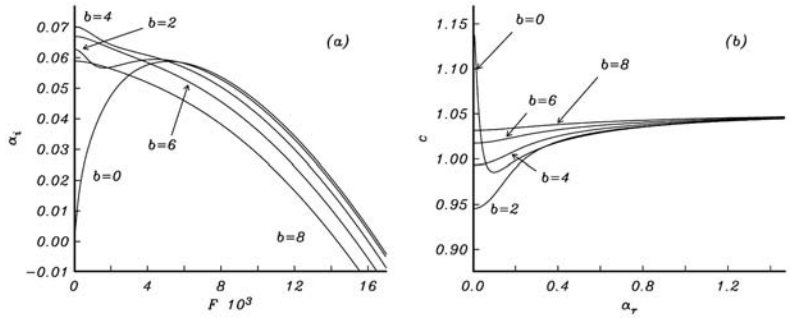

Figure 15—(a) Amplification curves for varying frequency for 3D disturbances at x = 0.224; R_δ =150; b = 1000, β/R_δ =for the mildly buoyant flow of U_e = 0.5 m/s. (b) The corresponding phase speed c variation with wavenumber α_r.

regime the 3-D disturbances are more destabilising than 2-D disturbances; with the stationary vortex being most unstable, while at high frequencies it is the 2-D disturbance that is most unstable. For stationary disturbances, we note from figure 15b that the streamwise wavenumbers are zero, and so these disturbances (the most dangerous from an instability viewpoint) are purely periodic in the spanwise direction only. Instability occurs over a finite range of β and at large enough β, disturbances return to being stable, while (though not shown) as $\beta \to 0$ the growth rates behave as $\alpha_t \sim \beta^{1/2}$.

The phase speed c, as ω (and thus α_r the wavenumber) tends to large values asymptotes to the maximum velocity overshoot value (in case shown this limit is ~ 1.05). This result is consistent with the Boussinesq based incompressible inviscid works of Mureithi and others (1997) and Denier and others (2001) who essentially build upon the more complete earlier, again Boussinesq based, asymptotic and numerical analysis of Hall and Morris (1993). The former two authors' findings were deduced primarily by a numerical solution to the 3-D version of the inviscid Taylor-Goldstein equation while our solutions are based at finite Reynolds number and allow for full compressibility, though for

the quite low external wind speeds considered the Mach number effects are insignificant. Their inviscid solutions suggest that the flow is unstable across the whole wavenumber spectrum and that growth rates become progressively larger as α increases and then state that viscosity ultimately must return the flow to a stable regime as $\alpha \to \infty$. Our viscosity included results confirm this result. They also confirm the findings of Hall and Morris (1993) that for nonzero β the mode with the largest growth rate occurs for $\omega = 0$. That is, the dominant wave mode becomes purely steady and two-dimensional in the spanwise direction, and at leading order the waves travel with a phase speed equal to the maximum of the streamwise velocity. This situation with the phase speed though only really arises in the limit of $\omega \to \infty$ in regions where our viscous included stability analysis, suggesting that disturbances have returned to a stable regime.

We only show neutral curves for values of Froude number down to $U_e = 0.5$m/s; this is merely for brevity, in that for even lower Froude numbers the instability envelope increases considerably, both in terms of the frequency space and even larger growth rates. An analogous result to figure 15 but corresponding to the highly buoyant flow at $U_e = 0.05$m/s is shown in figure 16. This merely confirms the findings deduced from the mildly buoyant case, in that decreasing Froude number increases the instability and unstable parameter space. We note from the eigenfunctions (fig. 17) the high frequency most amplified 2-D disturbance is localised off the wall about the position where the streamwise velocity attains its maximum overshoot value, while the purely spanwise periodic disturbance (fig. 17a) is situated close to the wall. This is clearly viscous in nature, while the former is of the inviscid type (fig. 17b). In the above, we only report on the first or most amplified mode, though as Reynolds number increases unstable higher modes were also identified.

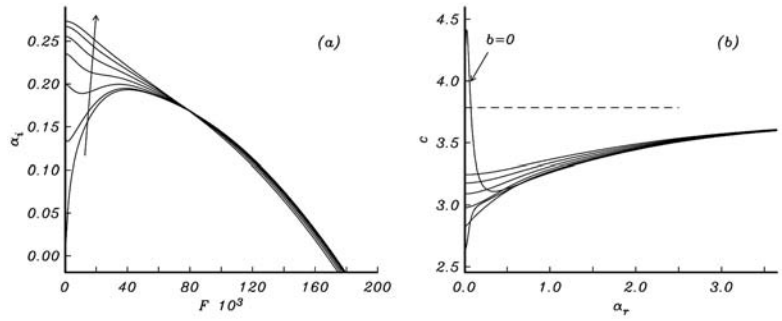

Figure 16—(a) Amplification curves for varying frequency for a number of 3-D disturbances (b = 0,(2),12) at $x = 0.169$, $R_\delta = 130$; b= 1000 β/R_δ for the highly buoyant flow of $U_e = 0.05$ m/s. (b) The corresponding phase speed c variation with wavenumber α_r. The dashed line corresponds to the maximum velocity overshoot value of ~3.78, as $\alpha_{rv} \to \infty$ the curves asymptote to this value.

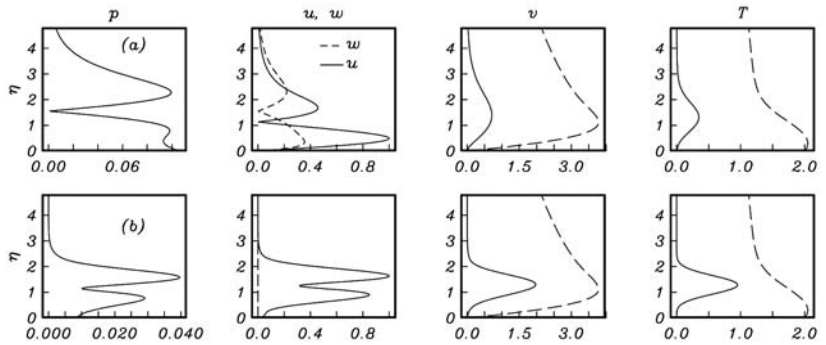

Figure 17— (a) Three-dimensional disturbance eigenfunctions computed for parameters of figure 16 at $F = 0$, $b = 12$, the pure vortex most amplified mode. (b) Two-dimensional eigenfunctions at $F = 120$, $b = 0$. The dashed curve in the v-plots is the overshot inflectional basic velocity profile, while the curve in the T-plot is the basic temperature profile.

Conclusions

We may conjecture that in the two Froude number limits, there are two different routes to fire behaviour and destabilisation, with the Froude number playing a crucial role in the boundary layer development and consequential instability of the convecting flow. The work lends support to some of the earliest criteria established (Byram 1954), and recently put forth by Nelson (2003), that erratic fire behaviour occurs when the ratio of the power of the wind to the power of the fire is ≤ 1 (essentially a Froude number definition). In view of the low growth rates in the high Froude number case, perhaps the significant factor is the sensitivity of the boundary layer to separate and lift off the wall; this being caused by massive updrafts of buoyant air. The relatively weak nature of instabilities in this regime suggests that the convecting boundary layer or fireline development would otherwise be well behaved. This is consistent with the work of Clark and others (1996b), who find that in high ambient windflows, a stable fireline arises forming a continuous parabolic shape (their model was fully three-dimensional and unsteady) as the fire evolves.

We have shown that the addition of heat goes directly into forming a highly accelerated streamwise velocity or jetlike flow in the low Froude number limit. In this limit, certainly the inflectional nature of profiles plays a strong role and must be a key feature in observed fire features. Local acceleration of flows by buoyancy and instability of inflectional profiles has been known about for some considerable time; however, its relevance in fire related problems has not been identified until now. The work suggests that if the ambient profile is initially inflectional, the transition to the unstable modes should be more rapid. The work essentially shows that a massive destabilisation via the inflectional route takes place in the low Froude number regime and that stationary, zero streamwise and nonzero spanwise wavenumber viscous disturbances have the highest growth rates. The results show that the flow can

support purely spanwise periodic disturbances (that is, vortices) and that it is feasible for these modes to have the largest growth rates. These are commonly referred to as pure vortex longitudinal "roll cell" modes. These might well be linked to cross roll features mentioned in the work of Cunningham and others (2003). Clark and others (1996b) identify similar features and state that a key requirement in breakup of the fireline is a low enough ambient wind (low Froude number) and thus speculate that the breakup is due to fire generated winds. Remarkably, in one of their figures, a distinct periodic spanwise vorticity field is seen, which they describe as *erratic* behaviour of the fireline.

In particular as regards the fingering phenomenon, Clark and others (1996b) hypothesise that once a fire line is long enough it cannot sustain a single convective updraft column and develops multiple columns due to long-line instabilities within the convection column. The convection attempts to form a long, vertically deep, nearly two-dimensional structure. Such two-dimensional structures are typically dynamically unstable due to either convective or shear instabilities and result in so-called cross-roll instabilities. Certainly fire-length (arising from a 3-D finite heat source) and side winds being drawn in may well play a role in the fingering phenomenon, but our analysis suggests that a possible mechanism might well be due or linked to the periodic spanwise stationary disturbances identified in our work. We find that it is the 3-D stationary disturbances that are the most unstable; these modes may have some bearing on the above description.

Acknowledgments

Part of this work was carried out while the first author was visiting the School of Computational Science at Florida State University. This work was supported by U.S. Department of Agriculture, Forest Service, Southern Research Station, Athens, GA, under a collaborative research agreement contract SRS 03-CA-11330136-056.

References

Banta, R.M.; Oliver, E.T.; Holloway, E.T.; Kropfli, R.A.; Bartram, B.W.; Cupp, R.E.; Post, M.J. 1992. Smoke column observations from two forest fires using Doppler Lidar and Doppler radar. J. Appl. Meteor. 31: 1328-1349.

Byram, G.M. 1954. Atmospheric conditions leading to blowup fires. Station Paper No. 35. Asheville, NC: U.S Department of Agriculture, Forest Service, Southeastern Forest Experiment Station.

Clark, T.L.; Jenkins, M.A.; Coen, J.; Packham, D. 1996a. A coupled atmosphere-fire model: Role of the Convective Froude number and dynamic Fingering at the fireline. Int. J. Wildland Fire 6(4): 177-190.

Clark, T.L.; Jenkins, M.A.; Coen, J.; Packham, D. 1996b. A coupled atmosphere-fire model: Convective feedback on fireline dynamics. J. Appl. Meteor. 35: 875-901.

Coen, J.; Mahalingham, S.; Daily, J. 2004. Infrared Imagery of Crown-Fire Dynamics during FROSTFIRE. J. Appl. Meteor. 43(9): 1241-1259.

Cunningham, P.; Hussaini, M.Y.; Goodrick, S.L.; Linn, R.R. 2003. Numerical simulations of buoyant plumes in a vertically sheared crossflow. Proceedings, American Meteorological Society Tenth Conference on Mesoscale Processes. Portland, OR. 3 p.

Daniels, P.G.; Gargaro, R.J. 1993. Buoyancy effects in stably stratified boundary layer flow. J. Fluid Mech. 250: 233-251.

Deardorff, J.W. 1973. The use of subgrid transport equations in a three-dimensional model of atmospheric turbulence. J. Fluids Eng. 95: 429-438.

Denier, J.O.; Stott, J.A.K.; Bassom, A.P. 2001. Three-dimensional inviscid waves in buoyant boundary layer flows. Fluid Dynamics Research. 28: 89-109.

Hall, P.; Morris, R. 1993. On the instability of boundary layers on heated flat plates. J. Fluid Mech. 245: 367-400.

Higuera, F.J. 1997. Boundary layer separation due to gas thermal expansion. Phys. Fluids. 9(10): 2841-2850.

Linn, R.R. 1997. A transport model for prediction of wildfire behaviour. Los Alamos National Laboratory Scientific Report. LA-13334-T, 195 pp. Los Alamos, NM.

Linn, R.R.; Cunningham, P. 2005. Numerical simulations of grass fires using a coupled atmosphere-fire model: Basic fire behaviour and dependence on wind speed. J. Geophysical Research. 110: D13107.

Morvan, D.; Dupuy, J.L. 2004. Modelling the propagation of a wildfire through a Mediterranean shrub using a multiphase formulation. Combustion and Flame 138: 199-210.

Mureithi, E.W.; Denier, J.P.; Stott, J.A.K. 1997. The effect of buoyancy on upper-branch Tollmien-Schlichting waves. IMA J. App. Math. 58: 19-50.

Noble, I.R.; Bary, G.A.V.; Gill, A.M. 1980. McArthur's fire-danger meters expressed as equations. Australian J. Ecology. 5: 201-203.

Nelson, R.M. Jr. 2003. Power of the fire—a thermodynamic analysis. Int. J. Wildland Fire. 12: 51-65.

Rothermel, R.C. 1972. A mathematical model for predicting fire spread in wild-land fuels. Gen. Tech. Rep. INT-115. Ogden, UT: U.S. Department of Agriculture, Forest Service, Intermountain Research Station.